Lifetime measurements of the $7p$ levels of atomic francium

J. E. Simsarian, L. A. Orozco, G. D. Sprouse, and W. Z. Zhao
Department of Physics, State University of New York, Stony Brook, New York 11794-3800
(Received 29 September 1997)

We present lifetime measurements of the $7p\,^2P_{3/2}$ and $7p\,^2P_{1/2}$ levels of Fr. We use a time-correlated single-photon counting technique on a cold sample of ^{210}Fr atoms in a magneto-optic trap. We excite the atoms with the trapping and repumping beams of the magneto-optic trap and detect the decay of the atomic fluorescence. The results are a precision experimental test of the atomic many-body perturbation theory applied to the heaviest alkali metal. The lifetime results are 21.02(11) ns and 29.45(11) ns for the $7p\,^2P_{3/2}$ and $7p\,^2P_{1/2}$ levels, respectively. This gives a line strength ratio $\mathcal{S}_{1/2}/\mathcal{S}_{3/2}$ of 0.526(3) for these levels in Fr. To study sources of systematic errors we measure the lifetimes of $5p\,^2P_{3/2}$ and $5p\,^2P_{1/2}$ in stable ^{87}Rb and obtain 26.20(9) ns and 27.64(4) ns, respectively. [S1050-2947(98)04504-1]

PACS number(s): 32.70.Cs, 31.15.Ar, 32.80.Ys

I. INTRODUCTION

The lifetime of a quantum mechanical system depends on the initial and final state wave functions and the interaction that connects them. Since the electromagnetic interaction in atomic physics is well understood, radiative lifetimes give information on atomic structure. The reliability of atomic theory calculations has been continually tested with alkali-metal atoms. They are the ''simplest'' atomic systems and recent measurements span a variety of techniques that, as in the case of Na, provide numbers that agree among themselves to better than $\pm 0.1\%$ [1–3]. The information extracted from atomic lifetime measurements can be of relevance to a wide variety of areas from astrophysics to lamp design. Of particular importance is the reliability of *ab initio* atomic theory calculations for the interpretation of fundamental measurements with atoms. Precise calculations are needed to extract weak force parameters from atomic parity nonconservation (PNC) experiments. Recent measurements of PNC in Cs [4] and Tl [5] put constraints on physics beyond the standard model. The Cs experiment also measured the nuclear anapole moment.

Among the heavy atoms francium is an excellent case to study. It is the heaviest alkali-metal atom and because of its large number of constituent particles, electron correlations and relativistic effects are important. Its large number of nucleons and simple atomic structure make it an attractive candidate for a future atomic PNC experiment [6]. The PNC effect is predicted to be 18 times larger in Fr than in Cs [7]. There has been considerable interest in measuring radiative lifetimes of the alkali-metal D_2 and D_1 levels to test the *ab initio* calculations. A result of the activity is the resolution of a prior discrepancy between the theoretical and experimental lifetimes in Li [8] and Na [1–3]. Recent measurements are now in agreement with the calculations.

In the absence of other decay paths, atomic radiative lifetime measurements give the square of the radial matrix element between two levels. The matrix elements have been calculated in Fr by Dzuba *et al.* [7] and Johnson *et al.* [9] using the techniques of many-body perturbation theory (MBPT). The same methods used for Fr have been applied to Cs. Our comparison of the measured matrix elements to the calculations tests their accuracy in a more complex system.

Atomic properties are sensitive to different ranges of the electron wave function. The radiative lifetime τ depends on the dipole moment operator $e\mathbf{r}$ spatially integrated with the wave functions and is most sensitive to large $\mathbf{r}$ properties. The PNC and hyperfine interactions depend on the electron wave functions at the nucleus, $\mathbf{r}\approx\mathbf{0}$. To extract information about the weak force from a PNC experiment that uses Stark interference, it is necessary to have both short-range (PNC, hyperfine) and long-range (τ, polarizability) knowledge of the electron wave functions.

Because there are no stable isotopes of francium, it is a difficult atom to study. References [10–13] give the experimental location of many atomic energy levels of Fr. Our lifetime experiments are the first measurements of atomic structure in Fr beyond transition energies. The powerful techniques of laser cooling and trapping have made this work possible.

In this paper we describe lifetime measurements of Fr and Rb atoms in a magneto-optic trap (MOT) . We measured the lifetimes of the $7p\,^2P_{3/2}$ and $7p\,^2P_{1/2}$ levels of Fr and the $5p\,^2P_{3/2}$ and $5p\,^2P_{1/2}$ levels of Rb and compare the Fr results to *ab initio* calculations. A preliminary report on our measurement of the $7p\,^2P_{3/2}$ and $5p\,^2P_{3/2}$ lifetimes appeared in Ref. [14]. As this work complements experiments in other alkali-metal atoms we summarize the present status of alkali-metal D_2 and D_1 lifetime measurements.

The paper is organized as follows. In Sec. II we discuss the *ab initio* calculations by Dzuba *et al.* and Johnson *et al.* We describe in Sec. III recent precision lifetime measurements in the alkali-metal atoms and consider the necessary experimental conditions for each. Section IV has a description of our method to measure the lifetime of radioactive Fr atoms in a magneto-optic trap. The data analysis for our experiment is in Sec. V with the results and conclusions in Secs. VI and VII.

II. *AB INITIO* CALCULATIONS IN FR

The works of Dzuba *et al.* [7] and Johnson *et al.* [9] use MBPT to calculate the atomic structure of francium to a high accuracy. The most complicated part of the method is calcu-

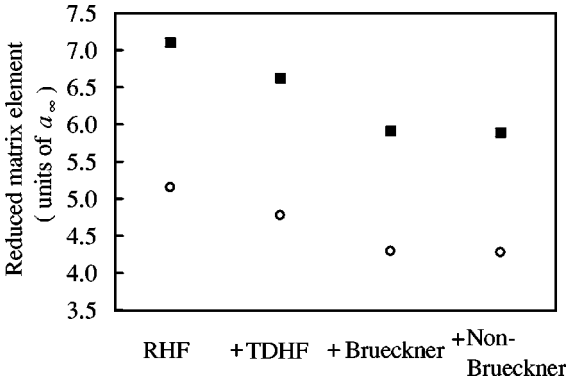

FIG. 1. Calculations of the reduced matrix elements in units of the Bohr radius (a_∞) for Fr $7P_{3/2}$ (boxes) and $7P_{1/2}$ (circles) by Dzuba *et al.* [7]. RHF is the relativistic Hartree-Fock result. TDHF includes core polarization. Brueckner includes electron correlations in the Brueckner approximation. Non-Brueckner includes additional corrections.

lating the interaction between the valence and the core electrons. The MBPT calculations predict the location of energy levels, hyperfine structure, radial matrix elements, and parity nonconserving transition amplitudes. These quantities are calculated from the MBPT atomic wave functions. Comparisons with experiments test the accuracy of the wave functions over different ranges of **r**.

Dzuba *et al.* begin with a relativistic Hartree-Fock (RHF) method to obtain a complete set of electron wave functions. They calculate the single-particle electron wave functions in the effective RHF potential as a perturbation expansion in terms of the difference between the exact and RHF Hamiltonians [15]. The relativistic equations automatically take into account the spin-orbit interaction. The time-dependent Hartree-Fock (TDHF) method gives the polarization of the core by the optical field. This changes the reduced matrix elements by -7% (see Fig. 1).

They calculate the states for the electron outside the core with the single-particle equation using the Brueckner approximation

$$(H_0+\Sigma)\psi=E\psi, \tag{1}$$

where H_0 is the relativistic Hartree-Fock-Dirac Hamiltonian, and Σ is the self-energy operator. The self-energy operator accounts for the correlation interaction of the valence electron with the core. Correlations arise from the Coulomb interaction between electrons in the many-body system. Dzuba *et al.* calculate lowest-order contributions to Σ for Fr. They also consider two classes of higher-order correlations: the hole-particle interaction and the screening of the Coulomb interaction. Screening factors from Cs account for these higher-order correlations in a semiempirical way.

Once they determine Σ they find the states of the external electron by iteratively solving Eq. (1) starting with the RHF wave functions. This method accounts for the dominating Brueckner-type correlation diagrams that correct the reduced matrix elements by $\approx -10\%$ (see Fig. 1). The non-Brueckner correlations are mostly from structural radiation and renormalization of the wave function, that are extrapolated from similar corrections in Cs. These modify the reduced matrix elements by -0.4%. The accuracy of the calculated reduced matrix elements in Fr by Dzuba *et al.* is expected to be $\pm 1\%$.

The RHF calculation of Johnson *et al.* [9] is in good agreement with that of Dzuba *et al.* The TDHF correction of Dzuba *et al.* is equivalent to the random phase approximation (RPA) correction of Johnson *et al.* [16]. The reduced matrix elements of the two groups differ slightly mostly from a difference in the Brueckner-type corrections. Johnson *et al.* calculated the corrections to third order and included fourth- and higher-order terms empirically. Since these terms play a significant role, it is expected that the result will not be as accurate as their ''all-order'' calculation in Cs [17]. The accuracy of the calculated reduced matrix elements in Fr by Johnson *et al.* is expected to be $\pm 2\%$.

III. EXPERIMENTAL METHODS

Precision lifetime measurements in the alkali-metal atoms use time-domain or frequency-domain techniques. The methods are complementary because they are sensitive to different systematic effects. Time-domain measurements include time-correlated single-photon counting and fast-beam experiments. Frequency-domain techniques include the measurement of the natural linewidth of the transition and measurement of the C_3 coefficient for diatomic molecules.

To get optimal information on the atomic wave functions there must be only one decay channel for the excited electron. The lifetime for an excited state with many decay channels is related to the sum over the different decay paths. Then it is more difficult to obtain information on the atomic wave functions.

A. Time-domain measurements

The most intuitive way to measure an atomic lifetime is to excite the atoms and record the exponential decay of the fluorescence as a function of time. Alternatively, a laser beam perpendicular to a fast atomic beam excites the atoms and detectors record the fluorescence as a function of distance from the excitation point. The velocity of the atomic beam and the distance determine the time of the fluorescence events.

It is important to have quantitative understanding of the measurement equipment. To measure a time interval, the time scale must be precisely calibrated. A fast-beam measurement requires accurate determination of the atomic beam velocity.

A difficulty of lifetime measurements in the time domain is the effect of quantum beats. Since a short pulse excites the atoms there can be coherence between the excited hyperfine or magnetic sublevels. Quantum beats cause a sinusoidal modulation of the exponential decay of the fluorescence. The splitting of the sublevels, the bandwidth of the excitation pulse, the polarization of the light, and the geometry of the detection determine the frequency and amplitude of the modulation.

1. Fast beam

The fast-beam technique utilizes an ion beam neutralized by charge-exchange collisions in a gas cell and is commonly

called beam-gas-laser spectroscopy. Typical beam energies range from 50 keV to 200 keV. Advantages of the method include good statistical quality of the data and small radiation trapping and quenching effects due to the low particle density of the atomic beam. A difficulty with the fast-beam measurements is the divergence of the atomic beam that results in a different light collection efficiency depending on the position of the fluorescence collection. Models of the beam divergence correct for this effect. Volz and Schmoranzer performed fast-beam measurements on the D_2 and D_1 lines of several alkali-metal atoms with precisions of $\pm 0.22\%$ in Li, $\pm 0.14\%$ in Na, $\pm 0.26\%$ in K, and $\pm 0.15\%$ in Rb [18]. Rafac *et al.* applied the technique to Cs with precisions of $\pm 0.23\%$ for the D_2 and $\pm 0.27\%$ for the D_1 lines [19].

2. Time-correlated single-photon counting

In time-correlated single-photon counting a laser repetitively excites the atoms and a fixed position detector collects the fluorescence as a function of time. The atoms move slowly so the solid angle for the fluorescence collection is nearly constant. The method relies on fast electronics to precisely record the time interval for detection events. Count rates are low to prevent dead-time effects in the electronics and to prevent preferential counting of early events. Low particle densities minimize radiation trapping and quenching effects due to collisions. Advantages of the method include good statistics and less sensitivity to the divergence of the atomic source.

Young *et al.* used a high-repetition-rate femtosecond, self-mode-locked laser to perform time-correlated single-photon counting on Cs atoms in a well-collimated atomic beam. Systematic uncertainties dominated the total measurement precisions of $\pm 0.33\%$ for the D_2 and $\pm 0.20\%$ for the D_1 lines [20].

Hoeling *et al.* measured the lifetime of the $5\,^2D_{5/2}$ level of Cs atoms in a vapor cell. A cw laser switched on and off with an acousto-optic modulator excited the atoms. Time-correlated single-photon counting of the detected 852 nm photons from the $6\,^2P_{1/2}$ decay to the $6\,^2S_{1/2}$ gave a lifetime measurement with $\pm 0.98\%$ precision [21]. Though cascade photons were detected in this measurement, the atoms decayed almost exclusively through the observed path. An important condition in this experiment was that the lifetime of the $6\,^2P_{1/2}$ is much shorter than the $5\,^2D_{5/2}$ level.

B. Frequency-domain measurements

1. Natural linewidth

The lifetime of an atomic transition results in a finite width of the resonance that is inversely proportional to the radiative lifetime. A measurement of the linewidth has different systematic limitations than time-domain experiments. The measurement requires a quantitative understanding of line-broadening mechanisms from sources such as the Doppler effect, saturation of the transition, and magnetic field inhomogeneities. Oates *et al.* [1] measured the line shape of velocity-selected cold Na atoms to obtain a D_2 lifetime with precision of $\pm 0.22\%$. Velocity selection reduced the Doppler broadening of the atoms that were precooled to 50 μK in an optical molasses. It was important to optically pump the atoms to effectively create a two-level system.

2. Photoassociative spectroscopy

A frequency-domain technique for lifetime measurement is the probing of the long-range portion of molecular potentials by photoassociative spectroscopy. A photoassociation photon induces two identical alkali-metal atoms to form a bound molecule. For Li, the highest levels of the $A^1\Sigma_u^+$ state were observed. For Na, K, and Rb the atoms form a molecule in the 0_g^- state that has a very large internuclear separation ($R_e = 2.76$ nm for K [22]). The long-range portions of the potentials are from a dipole-dipole resonant interaction with asymptotic behavior described by $V(R) = -C_3/R^3$. The coefficient C_3 is inversely proportional to the atomic radiative lifetime. A calculation of the interatomic potential is needed to extract C_3 from the photoassociation spectra. The high precision of the experiments and large separation of the atoms require inclusion of retardation effects in the calculation due to the finite speed of light. Fits of the calculated rovibrational eigenvalues to the experimental binding energies determine the C_3 coefficient. This method has been applied to D_2 and D_1 lines of cold alkali-metal atoms to achieve lifetime measurements with precisions of $\pm 0.03\%$ in Li [8], $\pm 0.10\%$ in Na [3], $\pm 0.19\%$ in K [22], and $\pm 0.23\%$ in Rb [23].

IV. LIFETIME MEASUREMENTS ON RADIOACTIVE FR ATOMS

Our technique to measure the $7p$ lifetimes of Fr efficiently utilizes the limited number of available radioactive atoms. Trapped atoms in a MOT are cold and well localized so each atom can scatter photons over many cycles. This is in contrast to an atomic beam experiment where each atom can scatter only one photon. Fast electro-optic modulators turn the trapping or repumping laser beams on and off to measure the lifetime of the atoms. A fixed photomultiplier tube detects the exponential decay of the fluorescence. Time-correlated single-photon counting of the fluorescence decay determines the lifetime. The method requires no lasers other than those necessary to trap Fr.

The MOT can also trap stable isotopes of Rb. We applied the same techniques to measure the lifetimes of the $5p\,^2P_{3/2}$ and $5p\,^2P_{1/2}$ levels of Rb. The measurements are an important test of the method and are interesting precision lifetime measurements in this atom. We studied systematic effects on the lifetime of Rb to establish bounds on systematic errors in Fr. We cannot be in the same room as the trap while we produce Fr due to fast neutrons from the nuclear reaction. The Rb measurements provide the opportunity to vary experimental parameters that are difficult to control remotely and to load a large number of atoms into the trap.

A. Trap for radioactive atoms

We capture Fr atoms in a MOT on line with the superconducting linear accelerator at Stony Brook. A beam of ^{18}O ions impinging on a Au target heated to 1200 K produces $\approx 1\times 10^6$/s ^{210}Fr that has a half-life of 3.2 min. By changing the ^{18}O beam energy we can selectively produce and trap

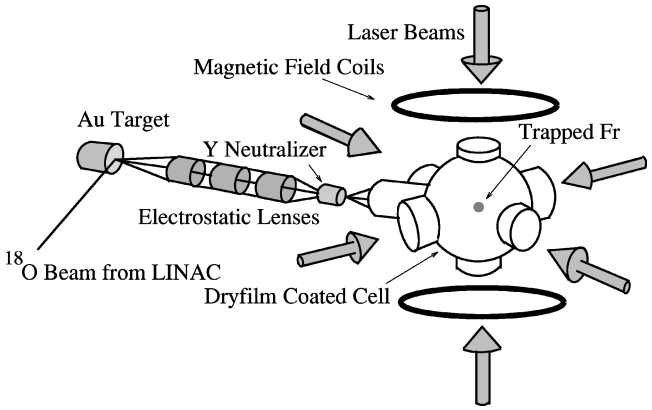

FIG. 2. Diagram of the apparatus for producing and trapping of Fr.

comparable quantities of ^{209}Fr, ^{210}Fr, and ^{211}Fr. The experiments reported here are done on ^{210}Fr. To obtain the low pressure necessary for MOT operation the Fr ions are moved from the Au target where they are created to a region of ultrahigh vacuum. We extract the Fr ions from the Au target through surface ionization. After an 800 V acceleration we focus the ions with electrostatic lenses and transport them to a Y foil heated to 1000 K. The Y foil releases neutral Fr atoms into the glass vapor cell where the MOT forms [6]. The background pressure in the MOT is $\leqslant 10^{-9}$ Torr (trap lifetime ≈ 20 s).

The system also contains a dispenser that can spray Rb atoms onto the surface of the target. The Rb follows the same path as Fr in our system. See Fig. 2 for a diagram of the apparatus that produces and traps Fr.

The vapor cell MOT for radioactive atoms requires a high trapping efficiency to collect the small number of atoms produced in the nuclear reaction. The trapping beams are large to provide trapping force over a substantial volume of the vapor cell. The trapping laser cools and confines the atoms on the cycling transition $7s\,^2S_{1/2},\ F=13/2 \rightarrow 7p\,^2P_{3/2},\ F=15/2$ (see Fig. 3). The cycling transition is not perfect and an additional laser repumps atoms that fall into the dark $7s\,^2S_{1/2},\ F=11/2$ state 46.7 GHz below $F=13/2$. The repumping can be accomplished with transitions to either the $7p\,^2P_{3/2}$ or $7p\,^2P_{1/2},\ F=13/2$ and we use the transition appropriate for the measurement (see Fig. 3).

The trapping laser is a Coherent 899-21 titanium sapphire (Ti:sapphire) laser with rms linewidth $\leqslant 500$ kHz. Six intersecting laser beams with $1/e^2$ (power) diameter of 4 cm and power of 80 mW form the MOT. The laser beam in each arm of the trap is retroreflected. The wave number of the trapping transition referenced to the I_2 spectrum is $13\,923.3866(26)\,\mathrm{cm}^{-1}$ [6].

The frequency of the trapping and repumping lasers drifts during data taking. We manually adjust the frequency of the lasers guided by a fluorescence image of the trap from a charge-coupled device (CCD) camera to keep the lasers on resonance. The wavemeter measures the wavelengths of the Ti:sapphire lasers and an I_2 absorption cell monitors the wavelength of the diode laser for the $7p\,^2P_{3/2}$ measurement. The Doppler broadened I_2 absorption features are too broad [full width at half maximum (FWHM) ≈ 2 GHz] to precisely locate the repumping transition. Frequency modulation of the diode repumping laser by 500 MHz at a rate of 4 kHz helps maintain the repumping resonance. For the $P_{1/2}$ lifetime measurements it is critical for the repumper laser to be very close to resonance. We adjust the repumper frequency to maximize the $P_{1/2}$ fluorescence.

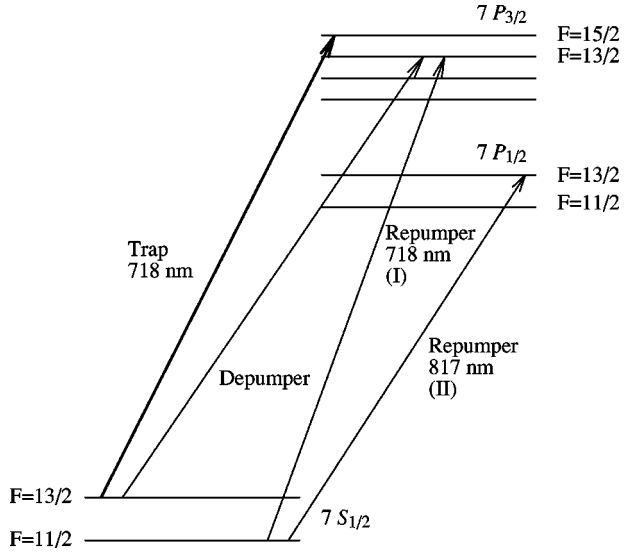

FIG. 3. Energy levels of ^{210}Fr relevant for trapping and lifetime measurements. Repumper (I) is a diode laser used for the $7P_{3/2}$ measurement. Repumper (II) is a Ti:sapphire laser used for the $7P_{1/2}$ measurement.

B. Atom excitation

The trapping and repumping lasers repetitively excite the atoms. They trap and excite the atoms during part of the cycle and are extinguished during the other part of the cycle to detect the fluorescence. To contain the atoms we make the trapping part a significant portion of the cycle. The lifetime measurements for the $P_{3/2}$ and $P_{1/2}$ levels require different excitation schemes.

The repetition rate for both measurements is 100 kHz. We choose the frequency of the cycle to minimize the loss of events due to the dead time of the electronics.

1. $P_{3/2}$ measurement

The trapping laser at 718 nm is the excitation source for the $7p\,^2P_{3/2}$ lifetime and passes through two Gsänger LM0202 electro-optic modulators (EOM) before entering the trap. We use two modulators to turn the light off cleanly and to get a large extinction ratio. The light turns on and off with a Gaussian $1/e$ (power) fall time of 9 ns and extinction ratio better than 800:1 (after 30 ns). A total of 260 mW of power passes through the modulators.

A free-running Mitsubishi 4405-01 diode laser cooled to 77 K repumps the atoms on the $7s\,^2S_{1/2},\ F=11/2 \rightarrow 7p\,^2P_{3/2},\ F=13/2$ transition at 718 nm. An acousto-optic modulator (AOM) turns the repumper off synchronously with the trapping laser to reduce the scattered light background. We measure no contribution to the background from the repumping laser while it is extinguished. Since the turn-off time of the acousto-optic modulator is slower than the electro-optic modulator, we extinguish the repumper

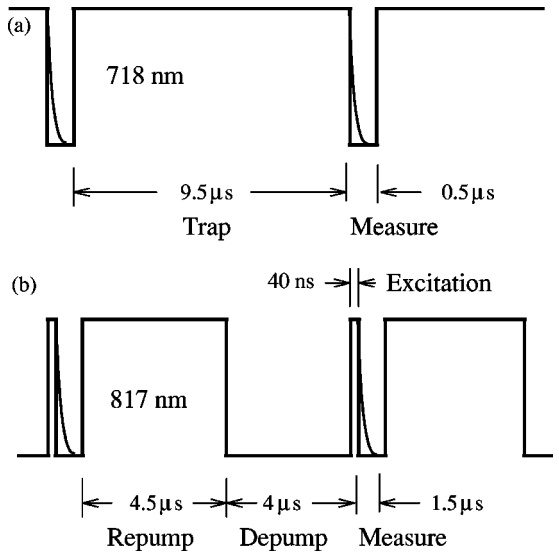

FIG. 4. Timing for the lifetime measurements. Curve (a) is the chopping of the 718 nm trapping and repumping lasers for the $7P_{3/2}$ experiment. Curve (b) is the chopping of the 817 nm repumping laser for the $7P_{1/2}$ experiment.

light before turning off the trapping laser. A 718 nm interference filter (bandwidth equal to 10 nm) in the detector assembly blocks background light from other sources.

The trapping and repumping lasers are on for 9.5 μs and we count 718 nm photons for 500 ns after the light is turned off [see Fig. 4(a)]. The chopping of the 780 nm trapping and repumping lasers is the same for the Rb $5p\,^2P_{3/2}$ measurement as for the Fr $7p\,^2P_{3/2}$ experiment.

2. $P_{1/2}$ measurement

The 718 nm trapping laser is continuously on for the $7p\,^2P_{1/2}$ measurement. A second Coherent 899 Ti:sapphire laser at 817 nm repumps the atoms on the $7s\,^2S_{1/2}$, $F=11/2 \rightarrow 7p\,^2P_{1/2}$, $F=13/2$ transition with total intensity of 17 mW/cm^2. The repumping laser, chopped with the EOMs, is the excitation laser for the $7p\,^2P_{1/2}$ lifetime measurement. The extinction ratio of the repumper is better than 250:1 with 20 mW of laser power. After passing through a fiber optic cable, 8.5 mW of repumper light are sent to the trap. The main trapping laser contributes little background counts due to the 817 nm interference filter (bandwidth equal to 1 nm) in the detector assembly. See Fig. 5 for a schematic diagram of the apparatus.

We estimate the population in the lower $F=11/2$ ground state to be at least 10^3 times lower than the $F=13/2$ state during normal MOT operation. Without transferring population to the lower ground state the fluorescence from the $7p\,^2P_{1/2}$ level is too small to be detected. As an initial attempt to transfer the population, we extinguished the repumper and moved the population to the lower ground state by leakage induced by the trapping laser at the trapping frequency. This method was not effective. As a way to actively transfer the population from the $F=13/2$ state to the $F=11/2$ ground state, we use an additional depumper beam tuned to the $7s\,^2S_{1/2}$, $F=13/2 \rightarrow 7p\,^2P_{3/2}$, $F=13/2$ transition (see Fig. 3). We derive the ^{210}Fr depumper from part of the trapping laser beam shifted down in frequency by 600 MHz

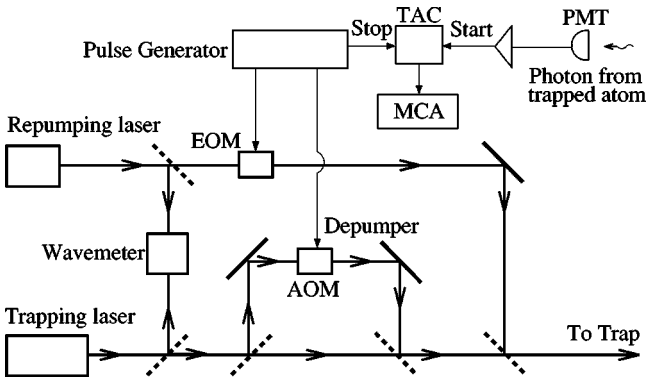

FIG. 5. Block diagram of $7P_{1/2}$ lifetime measurement apparatus.

with a double-passed acousto-optic modulator (Brimrose TEF-300). The depumper beam has an intensity of 0.4 mW/cm^2. A depumper beam is also necessary for the $5p\,^2P_{1/2}$ measurement in ^{87}Rb. We derive the ^{87}Rb depumper from the trapping laser with a double-passed acousto-optic modulator that shifts the laser frequency down by 250 MHz.

To measure the $7p\,^2P_{1/2}$ lifetime the repumper is on for 4.5 μs and is off for 4 μs. While the repumper is off, the depumping laser beam is on. Once significant population moves from the upper to the lower ground state, a short (40 ns) pulse from the repumping laser excites the atoms and we detect fluorescence at 817 nm for 500 ns [see Fig. 4(b)]. The chopping of the 780 nm depumping and 795 nm repumping lasers is the same for the Rb $5p\,^2P_{1/2}$ measurement as for the Fr $7p\,^2P_{1/2}$ experiment.

C. Fluorescence detection

There is a large amount of laser light scattered from the surfaces of the glass vapor cell while the trapping laser is on. Frequency modulation of the trapping laser with an amplitude of 4 MHz at a frequency of 14.5 kHz modulates the fluorescence amplitude of the trapped atoms. An $f/2$ optical system images the fluorescence onto a Hamamatsu R636-10 photomultiplier tube (PMT) and a lock-in detector demodulates it. The signal monitors the number of atoms in the trap during the measurements.

A second Hamamatsu R636-10 PMT operates in single-photon counting mode and detects fluorescence from the trapped atoms at an angle of approximately 45° from the vertical excitation lasers. This PMT detects the fluorescence for all the lifetime measurements. An $f/2$ optical system with an appropriate interference filter collects the fluorescence. A 1 mm diameter aperture at a focal point in the assembly rejects light spatially separated from the trapped atoms. This reduces the background and prevents saturation of the PMT. The overall detection efficiency is about 4×10^{-4}. The atoms move less than 0.1 μm during the measurement. There is no polarizer in the detector assembly.

We amplify and discriminate the pulses from the PMT before sending them to the pulse processing electronics. The rate of photon counts is low to prevent double pulse events and reduce dead-time systematic effects in the electronics.

D. Experimental considerations

A small number of atoms in the trap minimizes the effects of radiation trapping and collisional quenching of the excited state. Radiation trapping would lengthen the measured lifetime while collisional quenching would shorten it. We estimate the number of Fr atoms in the trap to be 1000 with a density of 10^6 atoms/cm^3.

There is a possibility of Zeeman quantum beats in the fluorescence signal. The spatially dependent restoring force in a MOT requires a magnetic field gradient in three dimensions. The magnetic field is on during the measurements. Varying the current to the field coils adjusts the gradient of the magnetic field. Currents of 40, 60, and 80 A correspond to magnetic field gradients of 3.7, 5.5, and 7.3×10^{-2} T/m. For equal intensity and polarization in all the trapping beams, the trap centers at the zero point of the magnetic field.

The EOM drivers produce large (350 V) voltage changes over short (9 ns) times resulting in rf radiation that can be received by the PMTs. We shield the cables to the detector until the background appears flat. The EOM drivers are in a different room than the PMTs for the $P_{1/2}$ measurements and in the same room as the PMTs for the $P_{3/2}$ measurements.

E. Data collection

The timing sequence for the chopping and detection comes from a Stanford Research S400 digital gate generator. The detection of a fluorescence photon from a trapped atom provides the start for an Ortec 467 time-to-amplitude converter (TAC) and a gate signal from the digital gate generator, synchronized with the EOM, provides the stop pulse (see Fig. 5). Starting the TAC with a fluorescence photon eliminates the accumulation of counts from cycles with no detected photons. A Canberra Series 35 Plus multichannel analyzer (MCA) bins the TAC output to produce a histogram of the events.

We quantitatively study the detection electronics to have a precise knowledge of their error contributions. There are uncertainties in the time scale and amplitude of the TAC and MCA combination. We calibrate the time scale of the TAC and MCA with a 9.4 MHz oscillator with a stability of 1×10^{-9}. A flashlight makes random pulses in the phototube that are gated with the oscillator. The gated pulses go to both the start and stop of the TAC. This produces randomly distributed events separated in time by an integer number of periods of the oscillator. The time calibration of the TAC and MCA has an uncertainty of $\pm0.04\%$. The time scale is linear to $\pm0.05\%$ over the entire range of channels with data.

For some data sets, the nonlinearity in the time scale of the TAC and MCA could be corrected by fitting the time calibration to a linear plus quadratic function. The fits after this correction modify the lifetime by $\pm0.01\%$. We measure the linearity in the height scale of the TAC and MCA with photons from a flashlight source that are randomly separated in time. The counts have a small linear deviation from a constant that could change the lifetime by 0.03%. The total uncertainty in the lifetimes from nonlinearity in the time scale and height scale of the TAC and MCA is $\pm0.03\%$. Each electronics unit has timing jitter of $<10\%$ of the TAC and MCA resolution. Tables I and II include these error contributions.

TABLE I. Error budget for the lifetimes of the D_2 and D_1 lines of Fr in percentage.

Error	Fr $P_{3/2}$(%)	Fr $P_{1/2}$(%)
Systematic		
TAC-MCA nonlinearity	±0.03	±0.03
Time calibration	±0.04	±0.04
Truncation error	±0.39	±0.19
Zeeman quantum beat	±0.04	±0.00
Other	±0.23	±0.25
Total systematic	±0.46	±0.32
Statistical	±0.24	±0.18
Sum in quadrature	±0.52	±0.37

We accumulate counts ($\approx1\times10^4$ fluorescence counts/channel) for about 20 minutes with atoms in the trap until the statistics are adequate [see Fig. 6(a)]. We then shift the trapping laser frequency off resonance so that there are no atoms in the trap and collect background for the same length of time. The background gives precise knowledge of the excitation function for the atoms [see Fig. 6(b)]. The 100 MeV ^{18}O beam is on the target while accumulating the background in case there are counts from radiation associated with the nuclear reaction. The subtraction of the background from the signal gives the exponential decay of the fluorescence for about five lifetimes [see Fig. 6(c)].

The statistical quality of the data is excellent. The signal-to-noise ratio at time 40 ns of Fig. 6(c) is 100. For the $7p\,^2P_{3/2}$ lifetime measurement the background count rate is 700 Hz mostly from dark counts and the imperfect extinction of the 718 nm laser. For the $7p\,^2P_{1/2}$ lifetime measurement the background count rate is 400 Hz mostly from dark counts and leakage of the 718 nm light through the 817 nm interference filter. The Rb results have similar background rates.

V. DATA ANALYSIS

Analysis of the fluorescence decay [see Fig. 6(c)] determines the atomic radiative lifetime. The details of the analysis follow. For Fr or Rb the results of the $P_{3/2}$ lifetimes will be presented first and the results of the $P_{1/2}$ lifetimes will follow in parentheses.

A. Correction for pulse pileup

A correction to the unsubtracted data accounts for the preferential counting of early events [24]. If N_i is the number

TABLE II. Error budget for the lifetimes of the D_2 and D_1 lines of Rb in percentage.

Error	Rb $P_{3/2}$(%)	Rb $P_{1/2}$(%)
Systematic		
TAC-MCA nonlinearity	±0.03	±0.03
Time calibration	±0.04	±0.04
Truncation error	±0.24	±0.11
Zeeman quantum beat	±0.21	±0.04
Total systematic	±0.32	±0.13
Statistical	±0.07	±0.08
Sum in quadrature	±0.33	±0.15

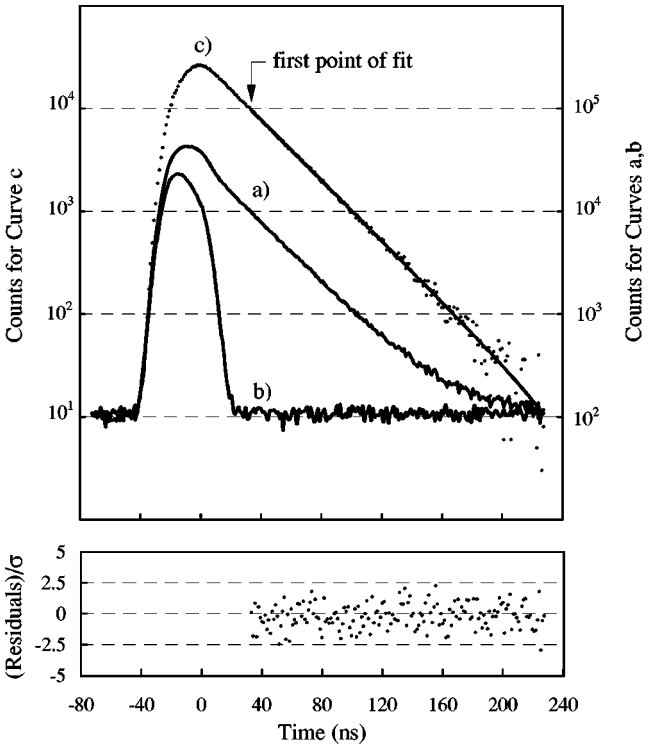

FIG. 6. Decay curves of Fr $7P_{1/2}$ level. Curve (a) is the raw data with Fr in the trap and curve (b) is the background. Curve (c) is the subtraction of a minus (b) and the straight line is a pure exponential fit to (c). The bottom shows the residuals of the fit divided by the statistical uncertainty of each point. The reduced $\chi^2=0.98$ for this measurement.

of counts in the MCA channel i, and N_E is the total number of excitation cycles, then N_A is the corrected number of counts in channel i given by

$$N_A=\frac{N_i}{1-(1/N_E)\sum_{j=1}^{i-1} N_j}. \tag{2}$$

Because low event count rates keep this correction small, we collect data with a small number of atoms in the trap. The correction alters the fitted lifetime of Fr by $+0.05\%(+0.04\%)$.

B. Fitting procedure

We subtract the background from the signal for each lifetime measurement and fit the fluorescence decay to the equation

$$N(t)=Ae^{-t/\tau}+B, \tag{3}$$

where the independent variable t is the MCA channel number. A least squares fitting algorithm determines the free parameters A, B, and the lifetime τ. We start the fits at a channel after the excitation light is off. This channel typically has 40% of the maximum number of counts. See trace (c) of Fig. 6 for an example of a fit. The residuals of the fit divided by the statistical uncertainty of each point are at the bottom of the figure. The standard deviation of the mean of the Fr lifetime is $\pm 0.24\%(\pm 0.18\%)$ (see Table I) and the average reduced χ^2 for all measurements is 1.01 (1.08). We apply the MCA calibration to τ after performing the fits.

The convolution of the light turn-off function with an exponential can account for the finite turn-off time of the excitation light. We fit the turn-off function of the light with a Gaussian and analytically perform the convolution with an exponential. This function allows fits to the data for times when the light is on. The results agree with the pure exponential fits for times when the light is off to within the statistical uncertainty. We report the result from the pure exponential fits as they involve fewer parameters.

C. Truncation uncertainty

There is a variation in the lifetime for fits over different ranges of the data. We define the point at half maximum on the falling edge of the excitation pulse to be time $t=0$. We vary the starting point of the fit from $t=23$ ns($t=20$ ns) to $t=34$ ns($t=43$ ns) and the end point of the fit from $t=257$ ns($t=203$ ns) to $t=366$ ns($t=317$ ns). The fitted lifetimes change over these ranges. We found no systematic trend to the fluctuation in the lifetimes. The truncation uncertainty is the standard deviation of the lifetime for the different starting and ending points of the fit. For Fr, an uncertainty of $\pm 0.39\%(\pm 0.19\%)$ accounts for the variation in the lifetime from the truncation of the fit [20]. This systematic uncertainty is the dominant error in the measurement of the $P_{3/2}$ levels (see Tables I and II).

We modeled the data by a pure exponential with Gaussian error distribution and performed the fitting procedure on the generated data. In this case the truncation uncertainty is three times smaller than the statistical uncertainty. This indicates that the experimental data has technical noise that increases the truncation error.

The truncation error is larger for the $P_{3/2}$ measurements than for the $P_{1/2}$ measurements on Fr and Rb. We carefully analyzed the fit residuals from the Fr $7p\,^2P_{3/2}$ and $7p\,^2P_{1/2}$ measurements. The residuals have larger deviations from zero in the $7p\,^2P_{3/2}$ experiment and the deviations are not repeatable for consecutive measurements. The technical noise may be from the PMT response to the rf radiation of the EOM drivers or from the amount of light the phototube detects. We expect the noise from rf radiation to be smaller for the $P_{1/2}$ measurements than for the $P_{3/2}$ measurements because of the location of the EOM drivers. However, the lack of repeatability of the noise suggests that it may be from a source other than rf radiation. The average number of counts is 5×10^{-2} counts/cycle for the $7p\,^2P_{3/2}$ measurement and is 5×10^{-3} counts/cycle for the $7p\,^2P_{1/2}$ measurement with similar numbers during the Rb experiments. There is a ten times higher count rate for the $7p\,^2P_{3/2}$ experiment because there is more scattered light from the longer and more intense excitation pulse. The higher count rate may introduce additional noise from the detection electronics.

D. Quantum beats

We have searched for quantum beats but have not observed any in the fluorescence signal. To have quantum beats a short laser pulse must coherently excite two closely spaced levels with energies E_1 and E_2 from a common lower level.

Then quantum interference between the excited levels modulates the total exponential decay of the fluorescence. To achieve coherent excitation with a laser pulse, the spectral bandwidth of the pulse must be greater than the frequency separation of the levels. Following the treatment by Demtröder [25], the total intensity of the emitted fluorescence with quantum beats as a function of time is

$$I(t)=Ce^{-t/\tau}\,[D+E\cos(\omega_{21}t)], \tag{4}$$

where $\omega_{21}=(E_2-E_1)/\hbar$. The coefficients D and E can be computed with the Clebsch-Gordan coefficients for the levels that produce the beats. The excitation and detection geometry of the experiment determine the spatial dependence of the quantum beats.

In contrast to experiments that use a mode-locked pulsed laser [20] with a large bandwidth we use a cw laser with bandwidth $\leqslant$500 kHz. The hyperfine splitting between the excited states of ^{210}Fr is 617 MHz (6.1 GHz). The 9 ns turn-off time of the EOM is too long to give enough laser bandwidth to coherently excite both hyperfine states. A Fourier transform of the fit residuals reveals no distinguishable components at the hyperfine splitting frequency.

We have considered the possibility of Zeeman quantum beats which would arise from coherent excitation of the excited hyperfine magnetic sublevels. A magnetic field shifts a hyperfine magnetic sublevel m_F in energy by $\Delta E=g_F\mu_B B m_F$ where g_F is the g factor for the level, μ_B is the Bohr magneton, and B is the external magnetic field. The energy shift determines the beat frequency.

A concern for this measurement are Zeeman beats with an oscillation period lower than the atomic lifetime as this could cause a systematic shift in the lifetime. The MOT requires a magnetic field gradient in three dimensions that is present during the measurements. The atoms at different locations in the trap experience different energy shifts. For balanced MOT beam intensities and polarizations, the trap center is at the zero of magnetic field. Our trap typically has a magnetic field gradient of 5.5×10^{-2} T/m and diameter of less than 1 mm so that an atom may be in a field of at most 2.8×10^{-5} T.

The MOT beams have both σ_+ and σ_- polarized beams. The different polarizations available from all the laser beams and different Larmor frequencies of the atoms tends to average out the effect of Zeeman beats when we count photons without a polarizer in front of the detector.

We have calculated the contribution of a Zeeman quantum beat to the lifetime of ^{210}Fr to give an upper limit to the systematic effect on the lifetime. We use a geometry that allows coherences between excited state m_F sublevels differing by two [26]. For a trap that forms at the zero of the magnetic field, the atoms are in a maximum field of 2.8×10^{-5} T. The expected beat frequency for these conditions is 209 kHz (40 kHz). In our calculation the fitted lifetime with this quantum beat is 0.04% (0.003%) shorter than from the decay free from quantum beats. We take this number as a systematic error (see Table I). The error for the $7p\,^2P_{3/2}$ is larger due to the five times larger value of g_F for this level compared to that of $7p\,^2P_{1/2}$.

To search for the effect of the magnetic field on the Fr lifetime we perform the measurements with magnetic field gradients of 3.7, 5.5, and 7.3×10^{-2} T/m. We observe no change in the lifetime to within the statistical uncertainty. Figure 7 graphs the measured lifetimes of Fr $7p\,^2P_{1/2}$ for three values of the magnetic field gradient. The error bars on the data are the statistical uncertainties. The larger error bar for the 3.7×10^{-2} T/m measurement is because there are fewer atoms in the trap. We performed the same set of measurements in Rb with no observable effect.

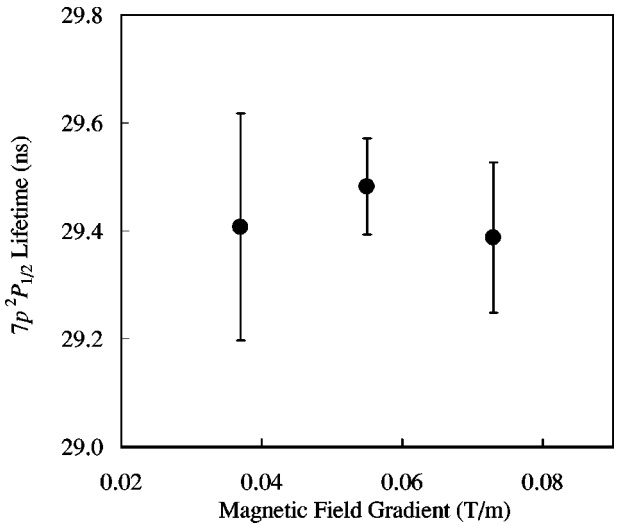

FIG. 7. Lifetime of $7P_{1/2}$ level in Fr for different trapping magnetic field gradients.

E. Systematic errors in Rb and Fr

An intensity or polarization imbalance in the trapping beams can result in the atoms not accumulating at the zero of the magnetic field. To test this we move the position ($\pm$ one trap diameter) of the trap by unbalancing the light in one arm of the trap, while keeping the detector fixed. We observe no systematic shift in the Rb lifetimes for these tests.

If the number of trapped atoms is large, the signal has an additional background of atomic fluorescence while the excitation laser is ''off'' due to imperfect extinction of the excitation light. Because we collect background with no atoms in the trap this results in counts in the signal that do not occur in the background and residual counts after subtraction. If the number of atoms in the trap is small, additional background fluorescence is not detectable and the subtraction has no residual counts.

With Rb in the trap, we decrease the number of atoms by decreasing the repumper power and increase the number by injecting more atoms into the trap from the Rb dispenser. The lock-in amplifier signal monitors the number of atoms in the trap. For measurements with a small number of atoms in the trap ($N\approx1000$) the subtraction has no residual counts and there is no systematic shift in the lifetime. For measurements with a large number of atoms in the trap ($N\approx100\,000$), the subtraction has residual counts. We include the constant B in the fitting function [Eq. (3)] to account for this. For measurements with a large number of residual counts ($B=400$ counts/channel for some measurements) the reduced χ^2 for the fits are as high as 3.0. The large reduced χ^2 for these fits indicates that the fluorescence

TABLE III. Summary of measured lifetimes in ns with comparisons to other measurements.

Author	Fr $P_{3/2}$	Fr $P_{1/2}$	Rb $P_{3/2}$	Rb $P_{1/2}$
Volz and Schmoranzer [18]			26.24(4)	27.70(4)
Heinzen and co-workers [23]			26.23(6)	
This work	21.02(11)	29.45(11)	26.20(9)	27.64(4)

decay is not well described by Eq. (3). This may be due to radiation trapping or collisional quenching of the excited state. The lifetimes of these measurements differ from the mean by as much as 0.8% and they are not included in the final determination of the Rb lifetime. Knowing the dependence of the lifetime on the number of atoms, we operate the trap in a region where there is no appreciable effect on the lifetime.

As another systematic test, we change the modulation amplitude of the trapping laser. For all the tests with a small number of atoms in the trap we find no appreciable effect on the Rb lifetimes within the uncertainty of $\pm 0.23\%(\pm 0.25\%)$ for a single data run. We conclude that all other systematic errors are smaller than this and we take it as an upper limit on other systematic errors in Fr (see Table I). The standard deviation of the mean lifetime of Rb is $\pm 0.07\%(\pm 0.08\%)$ and the truncation error of the fit is $\pm 0.24\%(\pm 0.11\%)$. The effect on the lifetime of a quantum beat [expected frequency of 523 kHz (129 kHz) in 2.8×10^{-5} T] calculated for ^{87}Rb is 0.21% (0.04%) and we add it as a systematic error.

The total uncertainty of the Fr (see Table I) and Rb (see Table II) measurements is a combination in quadrature of the contributions described above. This gives a total uncertainty of $\pm 0.52\%(\pm 0.37\%)$ for the Fr $7p\,^2P_{3/2}(7p\,^2P_{1/2})$ level and $\pm 0.33\%(\pm 0.15\%)$ for the Rb $5p\,^2P_{3/2}(5p\,^2P_{1/2})$ level. All errors are 1σ.

VI. RESULTS

The results of our lifetime measurements in Fr and Rb are shown in Table III. The Rb lifetimes are compared to the recent most accurate measurements of Volz and Schmoranzer that uses the fast-beam technique [18] and Heinzen and co-workers that uses photoassociative spectroscopy [23].

A. Radial matrix elements

From our measurements of the atomic lifetimes in Fr we determine the absolute value of the radial matrix elements for the transitions. The theoretical calculations determine their sign. The excited $7p\,^2P_{3/2}$ and $7p\,^2P_{1/2}$ levels have a single decay mode and the lifetimes are related to a single reduced radial matrix element between the excited and ground levels by

$$\frac{1}{\tau_{J'\to J}}=\frac{4}{3}\frac{\omega^3}{c^2}\alpha\frac{|\langle J\|r\|J'\rangle|^2}{2J'+1}, \tag{5}$$

where ω is the transition energy divided by $\hbar$, c is the speed of light, α is the fine-structure constant, J' and J are, respectively, the excited and ground state angular momenta, τ is the excited state lifetime, and $|\langle J\|r\|J'\rangle|$ is the reduced matrix element. Using the center of gravity of the experimentally measured transition energies from Ref. [10], the 21.02(11) ns [29.45(11) ns] lifetime gives 5.898(15) a_∞ [4.277(8)a_∞] for the absolute value of the $7s\,^2S_{1/2}\to 7p\,^2P_{3/2}$ ($7s\,^2S_{1/2}\to 7p\,^2P_{1/2}$) reduced matrix element, with a_∞ the Bohr radius.

The definition of the reduced matrix element used in this work [see Eq. (5)] is also used by Johnson *et al.* To convert the radial integral of Dzuba *et al.* to this convention multiply them by $\sqrt{(2J'+1)/3}$.

Figure 8 presents the graphical comparison between our measurements and the absolute value of the MBPT *ab initio* calculations [7,9] of the radial matrix element.

B. Line strength ratio

The atomic line strength ratio of the $J'=3/2$ and $J'=1/2$ levels reveals the large relativistic effects in the heavy Fr atom. The line strength of an atomic transition is given by

$$\mathcal{S}_{J'\to J}=\frac{|\langle J\|r\|J'\rangle|^2}{a_\infty^2}. \tag{6}$$

The line strength ratio for the $J'=3/2$ and $J'=1/2$ levels, $\mathcal{S}_{1/2}/\mathcal{S}_{3/2}$, is the ratio of the reduced matrix elements for the transitions and is independent of the transition energies. The dominant relativistic effect in the energy level structure of atoms is the spin-orbit interaction that results in the fine-structure splitting between the total angular momentum $J'=3/2$ and $J'=1/2$ levels. In the absence of fine-structure splitting the line strength ratio is simply the ratio of the sta-

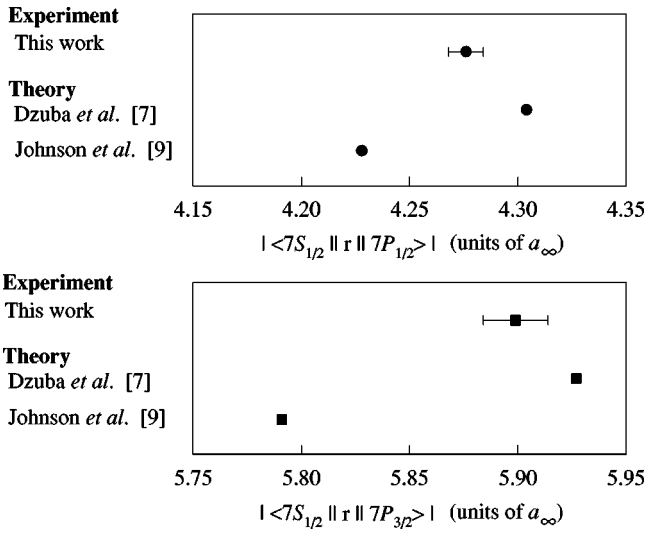

FIG. 8. Comparison of the absolute values of the $7S_{1/2}\to 7P_{1/2,3/2}$ transition radial matrix element with *ab initio* calculations from Refs. [7,9].

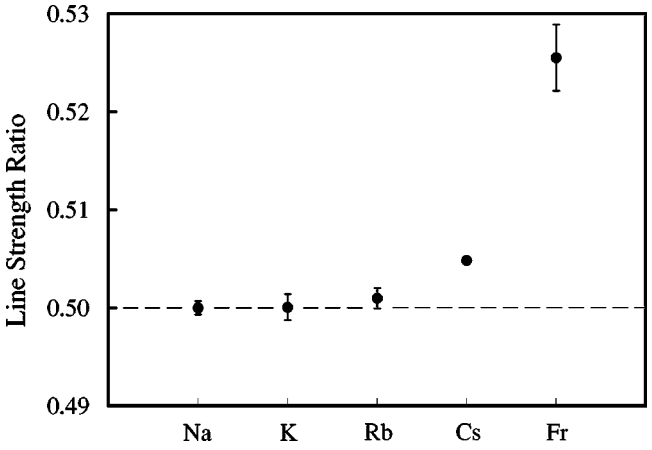

FIG. 9. Line strength ratio of alkali-metal atoms. Deviation from 0.5 indicates relativistic effects. The line strength ratios for the stable elements are measurements taken from Refs. [3,18,22,27].

tistical weights, $(2J'+1)$, of the two lines, 0.5. This is the case for the light alkali-metal elements where relativistic effects are small. The ratio increases for the heavier elements as relativistic effects become more important and the fine-structure splitting increases. Figure 9 plots the line strength ratio for the alkali-metal elements. The ratios for the stable elements were measured in Refs. [3,18,22,27]. Our result of 0.526(3) for $\mathcal{S}_{1/2}/\mathcal{S}_{3/2}$ for Fr shows a dramatic increase in relativistic effects over Cs [19,20]. The *ab initio* result of the calculations of $\mathcal{S}_{1/2}/\mathcal{S}_{3/2}$ for Fr by Dzuba *et al.* [7] is 0.527 and by Johnson *et al.* [9] is 0.533.

Relativistic effects enhance the PNC interaction in Fr. While the Z^3 scaling for the PNC interaction is only four times larger in Fr than Cs, the PNC effect in Fr is predicted to be 18 times larger than in Cs [7].

VII. CONCLUSION

We have measured the lifetimes of the first excited $P_{3/2}$ and $P_{1/2}$ levels of Fr and Rb. Our Fr measurements achieve excellent statistics and the results are limited by systematic uncertainties. We have demonstrated that laser cooling a relatively small number of atoms allows measurements with precisions comparable to experiments on stable atoms where many orders of magnitude larger samples are available. The results give new information about the atomic structure of the highly relativistic Fr atom. The agreement with the *ab initio* calculations indicates that PNC calculations in Fr with the same precision as Cs may be possible. We hope that our work encourages calculations of the atomic properties of Fr to a higher precision.

ACKNOWLEDGMENTS

We thank W. Shi, B. Gutiérrez, and D. Teaney for contributing to these measurements. We also thank T. Bergeman, H. Metcalf, S. L. Rolston, C. E. Tanner, and U. Volz for helpful discussions and equipment loans. This work was supported in part by a Precision Measurement grant from NIST and by NSF.

[1] C. W. Oates, K. R. Vogel, and J. L. Hall, Phys. Rev. Lett. **76**, 2866 (1996).
[2] U. Volz, M. Majerus, H. Liebel, A. Schmitt, and H. Schmoranzer, Phys. Rev. Lett. **76**, 2862 (1996).
[3] K. M. Jones, P. S. Julienne, P. D. Lett, W. D. Phillips, E. Tiesinga, and C. J. Williams, Europhys. Lett. **35**, 85 (1996).
[4] C. S. Wood, S. C. Bennett, D. Cho, B. P. Masterson, J. L. Roberts, C. E. Tanner, and C. E. Wieman, Science **275**, 1759 (1997).
[5] P. A. Vetter, D. M. Meekhof, P. K. Majumder, S. K. Lamoreaux, and E. N. Fortson, Phys. Rev. Lett. **74**, 2658 (1995).
[6] J. E. Simsarian, A. Ghosh, G. Gwinner, L. A. Orozco, G. D. Sprouse, and P. A. Voytas, Phys. Rev. Lett. **76**, 3522 (1996).
[7] V. A. Dzuba, V. V. Flambaum, and O. P. Sushkov, Phys. Rev. A **51**, 3454 (1995).
[8] W. I. McAlexander, E. R. I. Abraham, and R. G. Hulet, Phys. Rev. A **54**, R5 (1996).
[9] W. R. Johnson, Z. W. Liu, and J. Sapirstein, At. Data Nucl. Data Tables **64**, 279 (1996).
[10] For a sample and overview of the extensive work performed at ISOLDE see E. Arnold, W. Borchers, H. T. Duong, P. Juncar, J. Lermé, P. Lievens, W. Neu, R. Neugart, M. Pellarin, J. Pinard, J. L. Vialle, and K. Wendt, and the ISOLDE Collaboration, J. Phys. B **23**, 3511 (1990).
[11] S. V. Andreev, V. I. Mishin, and V. S. Letokhov, J. Opt. Soc. Am. B **5**, 2190 (1988).
[12] J. E. Simsarian, W. Shi, L. A. Orozco, G. D. Sprouse, and W. Z. Zhao, Opt. Lett. **21**, 1939 (1996).
[13] Z.-T. Lu, K. L. Corwin, K. R. Vogel, C. E. Wieman, T. P. Dinneen, J. Maddi, and H. Gould, Phys. Rev. Lett. **79**, 994 (1997).
[14] W. Z. Zhao, J. E. Simsarian, L. A. Orozco, W. Shi, and G. D. Sprouse, Phys. Rev. Lett. **78**, 4169 (1997).
[15] H. P. Kelly, Phys. Rev. **136**, B896 (1964).
[16] V. A. Dzuba, V. V. Flambaum, P. G. Silvestrov, and O. P. Sushkov, J. Phys. B **20**, 3297 (1987).
[17] S. A. Blundell, W. R. Johnson, and J. Sapirstein, Phys. Rev. A **43**, 3407 (1991).
[18] U. Volz and H. Schmoranzer, Phys. Scr. **T65**, 48 (1996).
[19] R. J. Rafac, C. E. Tanner, A. E. Livingston, K. W. Kukla, H. G. Berry, and C. A. Kurtz, Phys. Rev. A **50**, R1976 (1994).
[20] L. Young, W. T. Hill III, S. J. Sibener, S. D. Price, C. E. Tanner, C. E. Wieman, and S. R. Leone, Phys. Rev. A **50**, 2174 (1994).
[21] B. Hoeling, J. R. Yeh, T. Takekoshi, and R. J. Knize, Opt. Lett. **21**, 74 (1996).
[22] H. Wang, J. Li, X. T. Wang, C. J. Williams, P. L. Gould, and W. C. Stwalley, Phys. Rev. A **55**, R1569 (1997).
[23] H. M. J. M. Boesten, C. C. Tsai, J. R. Gardner, D. J. Heinzen, and B. J. Verhaar, Phys. Rev. A **55**, 636 (1997); D. J. Heinzen (private communication).

[24] D. V. O'Connor and D. Phillips, *Time Correlated Single Photon Counting* (Academic, London, 1984).

[25] W. Demtröder, *Laser Spectroscopy Basic Concepts and Instrumentation* (Springer-Verlag, Berlin, 1982).

[26] P. Schenck, R. C. Hilborn, and H. Metcalf, Phys. Rev. Lett. **31**, 189 (1973).

[27] R. J. Rafac, Ph.D. thesis, University of Notre Dame, 1997; R. J. Rafac and C. E. Tanner (unpublished).